Determination of L1157-B1 shock's proper-motions

Author: Marc Martí Aranda
Facultat de Física, Universitat de Barcelona, Diagonal 645, 08028 Barcelona, Spain.

Advisor: Gemma Busquet Rico

Abstract: This study investigates the proper motions of the B1 shock in the L1157 star-forming region, using two images of [SII] from the Nordic Optical Telescope obtained in two different epochs, in 2014 and in 2018. The goal was to enhance the understanding of shock dynamics by measuring the proper motions of knots within the shock structure, using cross-correlation technique. We identified a total of eight distinguishable knots. Our analysis revealed a general leftward movement in right ascension, while no clear trend was observed in declination. Notably, the most residual knots exhibited the highest velocities, pointing toward the nominal position of B1 protostellar shock, while those knots most linked to the collision remained stationary. The study highlights the need for extended observational periods to improve measurement precision.

I. INTRODUCTION

During the main accretion phase of protostellar evolution (i.e., Class 0 protostars), the star must maintain angular momentum while decreasing in size. To avoid reaching break-up speed, collimated jets and outflows are ejected to redistribute the angular momentum.

These jets and outflows have been observed in various star-forming regions, but certain aspects of their characterization remain uncertain, such as the ratio of ejected energy to accreted mass or whether these jets occur in all Class 0 protostars. Shock waves occur when the supersonic jets collide with the surrounding medium. These collisions compress and heat the gas, leading to the emission of radiation at various wavelengths. The study of these shocks provide insights into the physical conditions and processes occurring in star-forming regions.

In this study, we specifically examine the B1 shock generated by the Class 0 protostar in the L1157 cloud of the Cepheus Flare star-formation region. This region is particularly interesting due to its high presence of chemical elements. Particularly, it is the most chemically rich outflow known so far and contains elements such as SiO, NH_3, CH_3OH and H_2O among others [1].

L1157 is situated at an approximate distance of 352 ± 19 pc from Earth [2], making it an accessible object for detailed investigation. This distance has been obtained thanks to *Gaia* DR2 [3]. This outflow is excited by a cold, extremely red, young stellar object with a luminosity of $L = 11\ L_\odot$ [4]. Its low luminosity is a consequence of being still deeply embedded in their natal cloud. The base of the molecular jet was imaged for the first time by [5], who refined the precession jet model and estimated a dynamical age for the B1 shock of ≈1500 yr (adopting the new distance estimation).

FIG. 1 shows a general overview of the morphology of this outflow as well as the location of its main protostellar shocks. We can see that the B1 shock is the most prominent one.

With the aim of characterizing the B1 shock's proper motions, we used two different images of the [SII] atomic line obtained in two different epochs separated by four years.

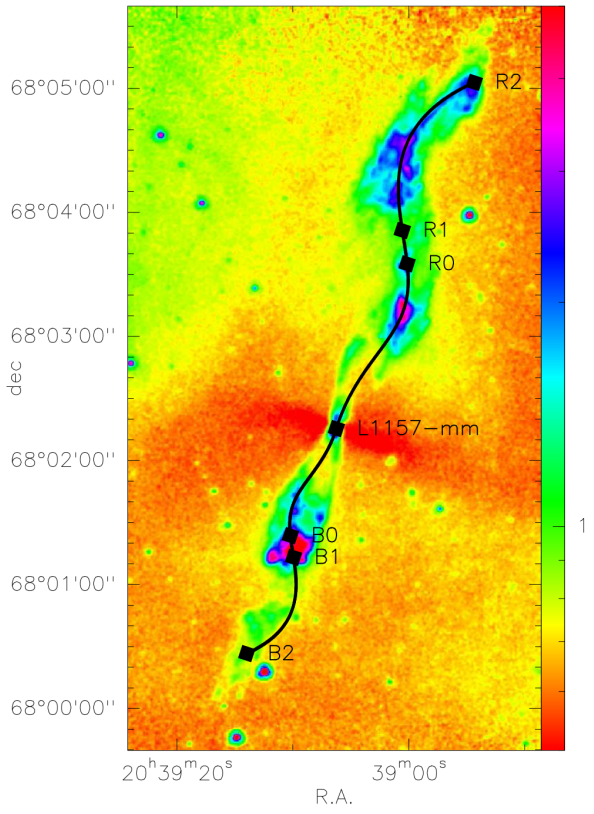

FIG. 1: *Spitzer*/IRAC 8 μm observations of the L1157 outflow. The resolution is ≈ 1.98″ and the intensity color scale is logarithmic from 0.05 to 5 mJy/sr. The precession model (black line) is overplotted. All shocks are marked. Figure from [5].

II. METHODOLOGY

A significant amount of useful information has been derived from the study of the B1 shock thanks to the Nordic Optical Telescope (NOT, [6]) located at the Observatorio del Roque de los Muchachos (La Palma, Spain).

We used the narrow-band filters of the Andalucía Faint Object Spectrograph and Camera (ALFOSC) centered at a wavelength of 6725 Å and with a bandpass of 50 Å to obtain images of the [SII] doublet. The field of view is 6.5×6.5 arcmin^2 and the image scale is 0.1896 arcsec pixel^{-1}. Images were taken in two different epochs, in August 2014 and August 2018. No calibration has been performed in this work as we obtained all data already calibrated.

A. Image alignment

The first step was to verify that both images were on the same reference system. For this we used IRAF software [7]. An examination of the specific locations of twenty-three well-known stars was undertaken. The results expected was that these stars would remain fixed and unchanged in both images, providing a constant point of reference. This technique enabled alignment verification of the two images in a common coordinate system.

B. Proper-motions determination

Once we had both images on the same reference system, we proceeded to determine the proper motions of the L1157-B1 shock. The method we used in this study is the cross-correlation.

Cross-correlation is a common statistical method used in astronomy to compare the similarity of two astronomical signals, usually light curves of celestial objects, based on their temporal (or spatial) offset. In mathematical terms, the cross-correlation R between two distinct discrete functions f and g is formally expressed as:

$$R_{fg}(m,n) = \Sigma_{i,j} f(i,j) \cdot g(i+m, j+n) \qquad (1)$$

where (i,j) are the indices of pixels and (m,n) are the displacements along x and y axes, respectively. The program's task is to calculate the highest correlation value by testing various displacements. It makes a parabolic fit to the cross correlation function to determine its peak and finally shows the displacement when the highest correlation is detected (see the description of the used method in [8]).

Cross-correlation stands out in observational astronomy for being able to determine the proper motions effectively [e.g., 8–10]. The cross-correlation method has several advantages over peak intensity analysis. First, it is more robust against noise because it looks at the overall relationship between signals globally, not just at specific peaks that can be easily distorted by random fluctuations. Second, by taking into account the entire shape of light curves, cross-correlation is able to pick up even subtle patterns that might indicate proper motion, without needing any obvious prominent peaks. Moreover, this method provides a quantitative measure of displacement that helps in accurately determining proper motions: this can be particularly useful when trying to detect minor motion or when uncertainties are high.

To determine the motion using cross-correlation, it is necessary to define regions (boxes) that contain each of the emission peaks or knots. In FIG.2 we show the boxes used to derive proper motions.

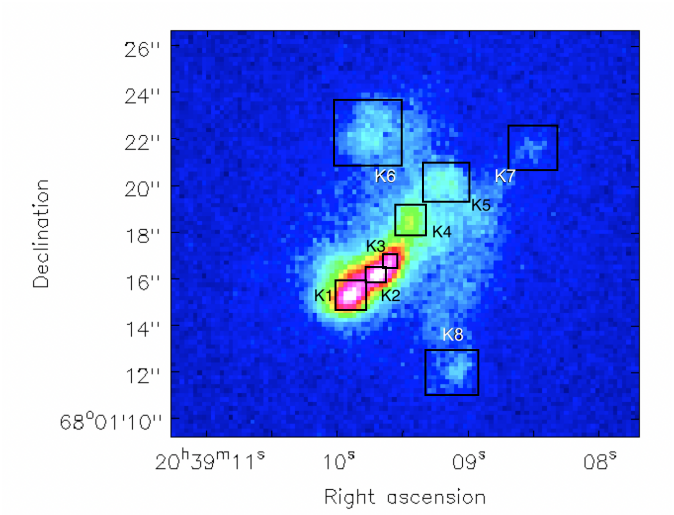

FIG. 2: [SII] image of the L1157-B1 shock captured in 2014. The boxes designed for deriving proper motions through cross-correlation are depicted and the corresponding knots are labeled.

III. RESULTS

We can see represented the contours of the [SII] emission of the two epochs in FIG. 3. The emission of [SII] consists of a bright knotty structure of $\sim 5'' \times 2''$ (1760×704 au at the distance of L1157), elongated along the southeast-northwest direction at P.A$\simeq$130°. This knotty structure is embedded in a more diffuse emission displaying a butterfly-like morphology with an angular extent of $\sim 15''$ ($\sim$ 5300 au). We identified 8 knots, labeled from K1 to K8 and selected a region box around each one (see FIG. 2) in order to derive the proper motions of each knot.

The cross-correlation measurement program considers an estimation of the error. This program conducts a thorough evaluation of the results within a ± 2 pixel range. By analyzing the variability of the results within this range, the program calculates the corresponding error.

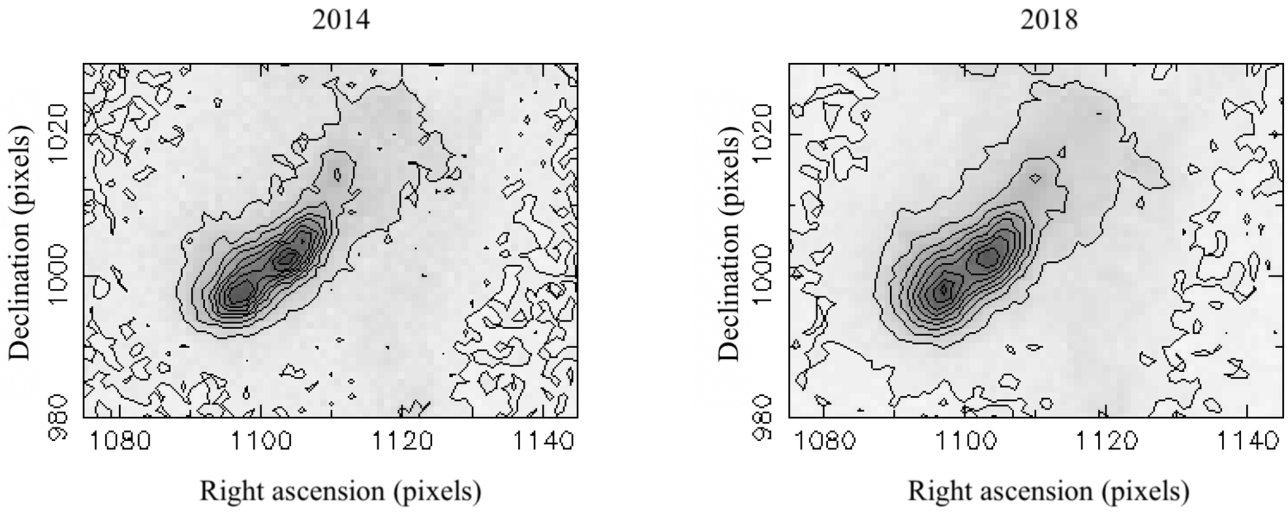

FIG. 3: The contours depicting data acquired from the atomic emission line of [SII] for both 2014 (left panel) and 2018 (right panel) are illustrated.

This method ensures a comprehensive assessment of potential discrepancies in the measurements.

We also measured the correlation of several stars close to the shock region to improve the accuracy of the error estimation. This approach provides more general information to obtain a more effective mean error analysis. In particular, we obtained mean errors of $\delta_x = 0.19$ pixels and $\delta_y = 0.13$ pixels for the right ascension and declination axes, respectively. These errors are under the pixel size, which verify that the alignment has been done properly. We also used the maximum error rate as a measure of accuracy. This conservative approach ensures that the reported proper motions account for the worst-case scenario in terms of measurement uncertainty.

We have all proper motions measured in terms of pixels. To derive the velocities of all knots we used the following expression:

$$v = 0.1896\Delta \frac{\pi}{648000} \frac{D}{t} \tag{2}$$

where 0.1896 is our resolution, Δ is the distance traveled in pixels, $\frac{\pi}{648000}$ is the conversion factor from arcsec to radians, D is the distance from Earth in kilometers and t is the time between the two images in seconds. The error of velocity is directly taken from equation 2 while the error of the total tangential velocity has been calculated using the following equation:

$$\delta v_t = \left|\frac{v_x}{v_t}\right| \delta v_x + \left|\frac{v_y}{v_t}\right| \delta v_y \tag{3}$$

where v_t is the tangencial velocity and v_x and v_y, the right ascension and declination velocities, respectively.

The proper motions derived are presented in Table 1. Below are the detailed description for each knot:

Knot K1: This knot exhibited a small leftward motion in the right ascension axis with a velocity of -12.26 ± 15.04 km/s. Given the substantial error margin, this motion is not statistically significant. However, the consistency with other knots' leftward motion suggests a possible collective movement pattern.

Knot K2: Similar to K1, K2 showed minimal movement. The measured velocity of -7.77 ± 15.04 km/s in the right ascension axis falls within the error margin, indicating no significant motion. The low velocity could be due to its proximity to the main shock front.

Knot K3: With a velocity of -10.44 ± 15.04 km/s, K3's motion also falls within the error margin. Its movement is consistent with the general leftward trend observed in the previous knots.

Knot K4: K4 exhibited a more substantial movement with velocities of -26.38 ± 22.64 km/s and -23.38 ± 33.25 km/s in right ascension and declination, respectively. Despite the higher velocities, the error margins remain large, making it difficult to draw definitive conclusions.

Knot K5: K5's movement was measured at -18.91 ± 15.04 km/s in the right ascension axis. This motion, while larger than K1-K3, still falls within a significant error margin, suggesting potential movement but requiring further observation for confirmation.

Knots K6, K7, and K8: These knots displayed the highest velocities, with K8 reaching -65.24 ± 20.01 km/s. Surprisingly, turned out to show the highest values

knot	Δ_x (pixels)	Δ_y (pixels)	μ_x (mas/year)	μ_y (mas/year)	v_x (km/s)	v_y (km/s)	v_t (km/s)
K1	-0.15 ± 0.19	0.09 ± 0.13	-7.34 ± 9.01	4.20 ± 6.16	-12.26 ± 15.04	7.01 ± 10.29	14.12 ± 18.16
K2	-0.10 ± 0.19	0.06 ± 0.13	-4.65 ± 9.01	2.94 ± 6.16	-7.77 ± 15.04	4.92 ± 10.29	9.20 ± 18.21
K3	-0.13 ± 0.19	0.02 ± 0.13	-6.25 ± 9.01	0.84 ± 6.16	-10.44 ± 15.04	1.41 ± 10.29	10.53 ± 16.28
K4	-0.33 ± 0.29	-0.30 ± 0.42	-15.80 ± 13.56	-14.00 ± 19.91	-26.38 ± 22.64	-23.38 ± 33.25	35.25 ± 39.00
K5	-0.24 ± 0.19	-0.06 ± 0.13	-11.32 ± 9.01	-2.76 ± 6.16	-18.91 ± 15.04	-4.61 ± 10.29	19.46 ± 17.05
K6	-0.08 ± 0.36	-0.78 ± 0.26	-3.97 ± 17.13	-37.16 ± 12.43	-6.63 ± 28.60	-62.05 ± 20.75	62.40 ± 23.68
K7	-0.37 ± 0.33	-0.44 ± 0.25	-17.56 ± 11.98	-20.88 ± 11.82	-29.33 ± 25.97	-34.87 ± 19.74	45.57 ± 31.82
K8	-0.82 ± 0.25	0.04 ± 0.20	-39.07 ± 11.98	1.68 ± 9.52	-65.24 ± 20.01	2.80 ± 15.90	65.30 ± 20.67

TABLE I: Proper motions measured in the L1157-B1 shock. The table includes the distance traveled in pixels, velocities in right ascension and declination, and the tangential velocity for all the knots identified in FIG 2.

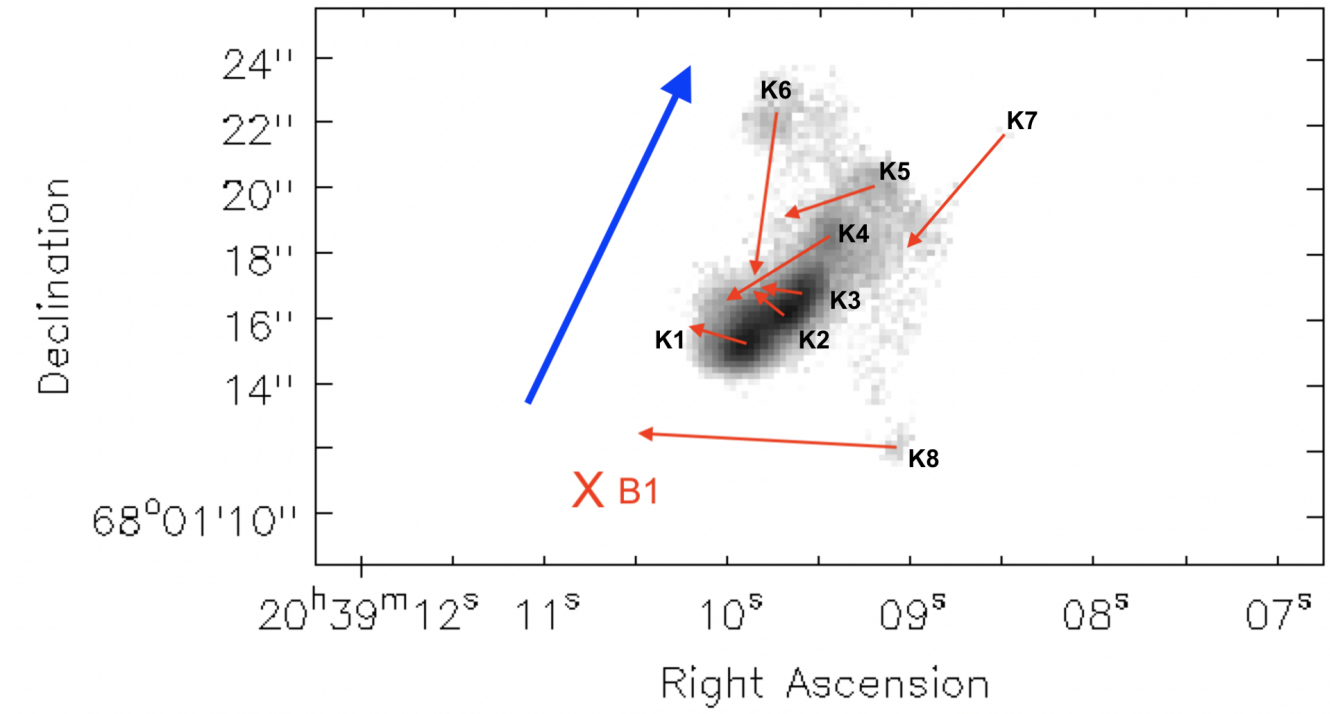

FIG. 4: Proper motions of each knot of the L1157-B1 shock. The arrows are not to scale; however, their lengths are proportional to the calculated tangential velocities. The cross represents the nominal position of B1 shock [1]. The blue arrow represents the direction of the protostelar and jet positions.

throughout the observation period. These knots are the faintest ones and are furthest from the impact region (see FIG. 4). A possible explanation of this result is that these knots present less prominent emission peaks so determining accurately their morphology is challenging. Small changes in morphology may be interpreted as substantial movements. Another explanation could be that the more residual nature of their emissions may result in their movement being more tangential compared to the primary shock front and they could even be influenced by a secondary shock wave. However, the most plausible explanation is that these knots are located in low-density areas, which could allow for greater movement, while the knots K1, K2, and K3 are in a high-density area, where movement is restricted.

Despite the error margins we can affirm that there's a clear general trend to the left in right ascension axe whereas there is not a clear general movement on the declination axes. This movement is coherent with the position from which the jet is ejected (see FIG. 4).

In summary, we can consider knots K1, K2, and K3 as stationary due to their low velocity and the fact that

their relative error is greater than 1 while the other 5 knots (K4, K5, K6, K7 and K8) seem to point toward a convergence point. This point is located near the nominal position of the shock (see FIG. 4).

Considering that the stars in the observed area should maintain a relatively fixed position over time with respect to the shock, the expected error in the movement of the stars should be the same regardless of the time elapsed. For the detected movements to exceed this calculated error, we need to obtain data over an interval of approximately 8 years.

As 10 years have passed since the first sample, current data would yield much more precise results with significantly smaller relative errors. Moreover, having data from three different epochs would reduce the error and provide more information about the morphological changes of knots K6, K7, and K8, determining whether the movements observed in this study are real or merely changes in the morphology of the emission.

Furthermore, with the aim to predict future positions and possible collisions with interstellar medium, it is necessary to study the spectroscopy of the region to obtain radial velocities.

IV. CONCLUSIONS

In this work, we analyzed the proper motions of the B1 shock in the L1157 molecular outflow, using two images of the [SII] atomic line obtained in 2014 and 2018.

We used the cross-correlation technique to determine these proper-motions and we identified eight individual knots in the general structure of the shock. Knots K1, K2, and K3 showed no significant movement, suggesting they are stationary. In contrast, knots K4, K5, K6, K7, and K8 exhibited more pronounced movements pointing to the nominal B1 shock position. The velocities of the knots are higher for the lower density areas, which indicates a vital role of the local environmental conditions.

While the current results are essential, further data pointing to a third epoch would significantly reduce the error we obtained and determine whether the observed motions are actual or possibly due to morphological changes. Future spectroscopic studies are crucial to record the radial velocities of the knots, which would complete the three-dimensional study and allow to make better predictions about their future evolution or collision with the interstellar medium.

V. ACKNOWLEDGMENTS

I would like to especially thank my tutor Gemma and Rosario for all the time and effort they have dedicated, their willingness and readiness to help at all times, and for all the knowledge they have shared with me. Thanks also to my friends and family, especially my mother, who has put up with me all this time. Without all of you, this work would not have been possible.

[1] Busquet, G., Lefloch, B.,"The CHESS survey of the L1157-B1 bow-shock: high and low excitation water vapor", A&A 561, A120, 2014.

[2] Zucker, C., Speagle, S., "A large catalog of accurate distances to local molecular clouds: the Gaia DR2 edition", ApJ 879, 125, 2019.

[3] Gaia Collaboration, Brown, A. G. A., Vallenari, A., "Gaia Data Release 2", A&A, 616, A1, 2018.

[4] Gueth, F., Guilloteau, S., "A precessing jet in the L 1157 molecular outflow", A&A 307, 891-897, 1996.

[5] Podio, L., Codella, C., "First image of the L1157 molecular jet by the CALYPSO IRAM-PdBI survey Astronomy", A&A 593, L4, 2016.

[6] The Nordic Optical Telescope, owned in collaboration by the University of Turku and Aarhus University, and operated jointly by Aarhus University, the University of Turku and the University of Oslo, representing Denmark, Finland and Norway, the University of Iceland and Stockholm University at the Observatorio del Roque de los Muchachos, La Palma, Spain, of the Instituto de Astrofisica de Canarias.

[7] IRAF is distributed by the National Optical Astronomy Observatories, which are operated by the Association of Universities for Research in Astronomy, Inc., under cooperative agreement with the National Science Foundation (`https://iraf-community.github.io/`).

[8] Anglada, G., López, R. et al. "Proper motions of the jets in the region of HH 30 and HL/XZ TAU: evidence for binary exciting source of the HH 30 jet", ApJ 132, 2799, 2007.

[9] López, R., Riera, A. et al. "The complex kinematical properties of the HH objects aligned with the HL Tauri and HH 30 outflows", MNRAS 282, 470-476, 1996.

[10] López, R., Estalella, R., "Collision of protostellar jets in the star-forming region IC 1396N: analysis of knot proper motions", A&A 661, 106, 2022.